INAF
ISTITUTO NAZIONALE
DI ASTROFISICA
NATIONAL INSTITUTE
FOR ASTROPHYSICS

Rapporti Tecnici INAF
INAF Technical Reports

Number	366
Publication Year	2026
Acceptance in OA@INAF	2026-02-05T15:00:42Z
Title	X-ray follow-up work on a set of unassociated sources listed in the Palermo Swift/BAT 100-month catalogue
Authors	LANDI, RAFFAELLA, Bassani, Loredana
Publisher's version (DOI)	https://doi.org/10.20371/INAF/TechRep/366
Handle	http://hdl.handle.net/20.500.12386/45321

X–ray follow–up work on a set of unassociated sources listed in the Palermo *Swift*/BAT 100–month catalogue

Raffaella Landi & Loredana Bassani

(INAF – OAS Bologna)

Introduction

In the following, we provide a report on a preliminary study aimed at searching the X–ray counterpart to a set of still unassociated sources listed in the Palermo *Swift*/BAT 100–month catalogue (available at: `http://bat.ifc.inaf.it/100m_bat_catalog/100m_bat_catalog_v0.0.htm`). By exploiting the capability of the X–ray telescope (XRT, 0.2–10 keV) onboard the Neil Gehrels *Swift* Observatory (Gehrels et al. 2004) to localise the sources with a positional accuracy of few arcseconds, the search for optical/UV, infrared, and radio counterparts is more efficient and reliable. Each source is discussed in a dedicated section in which we report the log of the XRT observations, the likely counterparts detected, their spectral behaviour, and their multi–wavelength properties.

The *Swift*/BAT sources discussed in this report are the following:

- 4PBC J0200.8+5423
- 4PBC J0258.8+3544
- 4PBC J0304.6–3026
- 4PBC J1626.4–3329
- 4PBC J1630.0+2680
- 4PBC J1638.8–1413
- 4PBC J1735.9–1528
- 4PBC J1824.5+2054
- 4PBC J2201.3+7546

Swift/XRT data reduction and analysis

XRT data reduction was performed using the standard data pipeline package (*xrtpipeline* v. 0.13.6), in order to produce screened event files. All data were extracted only in the Photon Counting (PC) mode (Hill et al. 2004), adopting the standard grade filtering (0–12 for PC) according to the XRT nomenclature.
We then, in case of multiple observations, summed together all the available XRT pointings using *XSELECT* v. 2.4m to enhance the signal–to–noise ratio and thus facilitate the detection of candidate counterparts. As a following step, we analysed the XRT images in the 0.3–10 keV energy band by means of *XIMAGE* v. 4.5.1 in search of X–ray detections within the 95% BAT error circles. The position of the brightest X–ray detections were estimated by using the task *xrtmkarf* v. 0.2.9; for weaker sources we made use of the *XIMAGE* command *detect*. In the XRT images, the black circles depict the 95% BAT positional uncertainties as reported in the 100–month Palermo *Swift*/BAT catalogue.
To visualise better the X–ray counterparts, we smoothed the images. Therefore, the presence of grains and/or features inside the XRT field of view is undoubtedly spurious; in some cases the poor quality of the XRT images is due to the low exposure.
Source events were extracted from the corresponding event file within a circular region with a radius of 20 pixels (1 pixel corresponding to 2.36 arcseconds) centred on the source position; if

the source is bright, a 30–pixel radius may be a more suitable choice. Background events were extracted from a source–free region close to the X–ray source of interest. Then, the source spectra were extracted using the *XSELECT* v. 2.4m software and generally binned using *grppha* to 20 counts per energy bin so that the χ^2 statistic could be applied. For sources with fewer counts (typically lower than 50), data were binned to 1 count per energy bin and the Cash statistic (Cash 1979) was adopted. We used version v. 016 of the response matrices and created individual ancillary response files arf using *xrtmkarf* v. 0.6.3. The spectral analysis was performed using *XSPEC* v. 12.12.0.
In the first instance, we adopted a basic model consisting of a simple power law passing through Galactic absorption in the source direction (Kalberla et al. 2005). If this baseline model was not adequate to fit the data, we then introduced extra spectral components as required.

The multi–wavelength properties of the objects analysed in this work were collected by exploiting various catalogues and databases reported in the following list:

- The United States Naval Observatory B–1.0 Catalogue (USNO B–1.0, Monet et al. 2003);
- The United States Naval Observatory A–2.0 Catalogue (USNO A–2.0, Monet 1998);
- The Two Micron All–Sky Survey (2MASS, Skrutskie et al. 2006);
- Two Micron All Sky Survey Extended Source Survey (2MASX, Skrutskie et al. 2006);
- The Third *Gaia* Data Release, *Gaia* EDR3 (Gaia Collaboration 2021);
- The Wide–field Infrared Survey Explorer (WISE, Wright et al. 2010);
- The AllWISE Source Catalogue (Cutri et al. 2013);
- The Galaxy Evolution Explorer All–Sky Survey (GALEX, Bianchi et al. (2011);
- The Six–degree Field Galaxy Survey (6dFGS, Jones et al. 2009);
- The Dark Energy Spectroscopic Instrument (DESI) Legacy Imaging Surveys DR8 photometric redshifts (Duncan 2022);
- The Dark Energy Camera Plane Survey (DECaPS, Schlafly et al. 2018);
- The Panoramic Survey Telescope and Rapid Response System (Pan–STARRS, Chambers et al. 2016);
- The *XMM–Newton* Slew Survey Full Source Catalogue (XMMSL1, Saxton et al. 2008 and relative updates);
- The Specktr–RG (SRG)/*eROSITA* All–Sky Survey (eRASS1) (Merloni et al. 2024);
- The *ROSAT* All–Sky Survey Bright/Faint Source Catalogues (Voges et al. 1999);
- The National Radio Astronomy Observatory (NRAO) Very Large Array (VLA) Sky Survey (NVSS, Condon et al. 1998);
- The Very Large Array (VLA) Faint Images of the Radio Sky at Twenty–centimeters (FIRST) Survey (Helfand et al. 2015);

- The Sydney University Molonglo Sky Survey (SUMSS V2.1, Mauch et al. 2003);
- The Giant Metrewave Radio Telescope All–Sky 150 MHz Radio Source Catalogue (Intema et al. 2017);
- The Rapid Australian SKA Pathfinder (ASKAP) Continuum Survey (RACS). V. RACS–mid 1367.5 MHz Catalogue (Duchesne et al. 2024);
- The Rapid Australian SKA Pathfinder (ASKAP) Continuum Survey (RACS). VI. RACS–high 1655.5 MHz Catalogue (Duchesne et al. 2025);
- The Karl G. Jansky Very Large Array Sky Survey (VLASS, Lacy et al. 2020);
- The Very Large Array Sky Survey (VLASS) QL Ep.1 Catalogue, CIRADA version (Gordon et al. 2021);
- The GaLactic and Extragalactic All–Sky Murchison Widefield Array eXtended (GLEAM–X, Ross et al. 2024);
- The MeerKAT Absorption Line Survey (MALS). I. DR1 (Deka et al. 2024);
- The NASA/IPAC Extra Database (NED), available at: `https://ned.ipac.caltech.edu/`;
- The VizieR Catalogue Service, available at: `https://vizier.cds.unistra.fr/viz-bin/VizieR`;
- The High Energy Astrophysics Science Archive Research Center provided by NASA's Goddard Space Flight Center (HEASARC), available at: `http://heasarc.gsfc.nasa.gov/`;
- The SIMBAD Astronomical Database, available at: `http://simbad.u-strasbg.fr/simbad/`.

The method we adopted to pinpoint the unidentified sources that are likely to be Active Galactic Nuclei (AGNs) is based on diagnostic indicators such as *WISE* colours, radio emission, and indication of extension in the optical images (see details in Malizia et al. 2023).

4PBC J0200.8+5423

Source position:

- R.A.(J2000) = $02^{h}00^{m}54'.00$
- Dec.(J2000) = $+54^{\circ}23'20''.40$
- Positional uncertainty = $2'.88$

Six XRT observations available:

1. obscode: 00085287001
   observation date: 06/11/2014
   exposure: 196 s
2. obscode: 00085287002
   observation date: 07/11/2014
   exposure: 228 s
3. obscode: 00085287003
   observation date: 13/11/2014
   exposure: 128 s
4. obscode: 00085287004
   observation date: 15/11/2014
   exposure: 363 s
5. obscode: 00085287005
   observation date: 17/11/2014
   exposure: 1138 s
6. obscode: 00085287006
   observation date: 18/11/2014
   exposure: 732 s

XRT detects two X–ray sources in the region surrounding 4PBC J0200.8+5423 (see Figure 1):

➢ Source #1 lies within the BAT positional uncertainty and is located at:

R.A.(J2000) = $02^{h}00^{m}58'.37$

Dec.(J2000) = $+54^{\circ}23'46''.70$

error box = $4''.60$

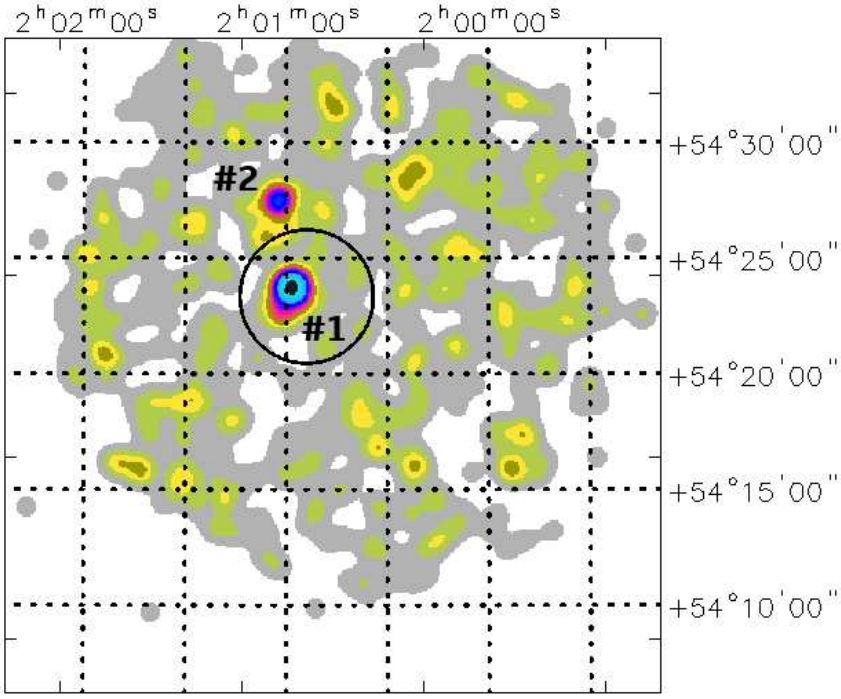

Figure 1: 0.3–10 keV XRT image of the 4PBC J0200.8+5423 field.

It is detected at 6.5σ c.l. in the 0.3–10 keV energy band and at 5.5σ c.l. above 3 keV.

Multi–wavelength counterparts to this XRT detection:

- USNO–A2.0 1425–02787694 with magnitudes $B = 13.5$ and $R = 11.5$;
- 2MASS J02005845+5423423 with magnitudes $J = (12.671 \pm 0.061)$, $H = (11.906 \pm 0.067)$, and $K = (11.603 \pm 0.054)$;
- 2MASX J02005846+5423427 with magnitudes $J = (11.904 \pm 0.021)$, $H = (11.209 \pm 0.030)$, and $K = (10.789 \pm 0.029)$;
- AllWISE J020058.44+542342.2 with magnitudes $W1 = (10.788 \pm 0.023)$, $W2 = (10.597 \pm 0.021)$, $W3 = (8.276 \pm 0.022)$, $W4 = (5.797 \pm 0.037)$, and colours not so typical of an AGN candidate ($W1 - W2 = 0.191$, $W2 - W3 = 2.321$);
- *Gaia* 456365740065814272 with magnitudes $G = (18.748 \pm 0.058)$, $BP = (15.954 \pm 0.049)$, and $RP = (14.322 \pm 0.026)$
  ($BP - RP = 1.632$);
- VLASS1QLCIR J020058.42+542342.3 with flux Ftot(2000–4000 MHz) $= (7.788 \pm 0.289)$ mJy.

From the XRT data we infer a 2–10 keV flux of $\sim 3.4 \times 10^{-12}$ erg cm^{-2} s^{-1} by assuming a power law continuum, with photon index $\Gamma = \left(-0.33^{+0.45}_{-0.49}\right)$, passing through Galactic absorption ($N_{\rm H(Gal)} = 1.78 \times 10^{21}$ cm^{-2}). If we freeze the photon index to 1.8, the data show evidence, although the poor statistics, of extra absorption $N_{\rm H(int)} = \left(2.79^{+1.84}_{-1.15}\right) \times 10^{22}$ cm^{-2};

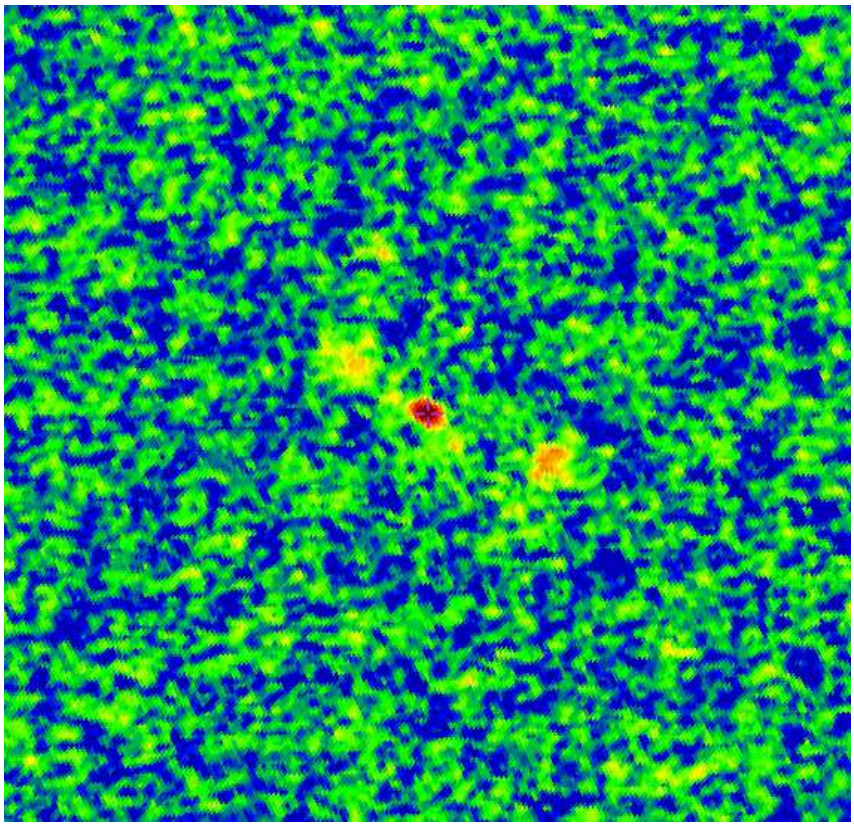

Figure 2: Radio image of source #1 from VLASS.

the 2–10 keV flux is $\sim 1.8 \times 10^{-12}$ erg cm^{-2} s^{-1}.

The source is identified with LEDA 2468432, an AGN candidate at redshift $z = (0.016104 \pm 0.000037)$. It is variable in radio at 1.4 GHz from the comparison between NVSS and FIRST data sets (Ofek et al. 2011); the source radio morphology from VLASS may be that of a radio galaxy with a bright central core and two dim opposite lobes (see Figure 2). The total extension is around $1'$ or 20 kpc (0.330 kpc/arcseconds), suggesting a young radio galaxy. We also note that the source *AllWISE* colours are more typical of either a heavily absorbed AGN (which is not suggested by the low column density measured in X–rays) or of a low–luminosity/low–excitation AGN like a Low–Ionization Nuclear Emission–line Region (LINER) (see Dabhade et al. 2020 for a classification of the various AGN types on the basis of near–infrared colours). Optical spectroscopy will eventually shed light on the true nature of this source.

➢ Source #2 falls outside the BAT error circle and is located at:

R.A.(J2000) = $02^{\rm h}01^{\rm m}02'.53$

Dec.(J2000) = $+54^{\circ}27'28''.20$

error box = $6''.00$

It is detected at 3.4σ c.l. in the 0.3–10 keV energy range; no detection is found above 3 keV.

Multi–wavelength counterparts to this XRT detection:

- USNO–A2.0 1425–02789418 with magnitudes $B = 19.3$ and $R = 19.3$;
- AllWISE J020102.12+542732.1 with magnitudes $W1 = (13.251 \pm 0.025)$, $W2 = (13.091 \pm 0.030)$, $W3 = (11.338 \pm 0.182)$, $W4 = (8.565 \pm 0.328)$, and colours again not so typical of an AGN candidate ($W1 - W2 = 0.16$, $W2 - W3 = 1.75$);
- *Gaia* 456366491682644224 with magnitudes $G = (19.476 \pm 0.008)$, $BP = (19.508 \pm 0.038)$, and $RP = (18.946 \pm 0.033)$
  ($BP - RP = 0.562$).

From the X–ray data we can only estimate a 2–10 keV flux of $\sim 2.3 \times 10^{-13}$ erg cm^{-2} s^{-1} by assuming a power law passing through Galactic absorption ($N_{\mathrm{H(Gal)}} = 1.79 \times 10^{21}$ cm^{-2}) with the photon index frozen to 1.8.

This source is weaker and softer than object #1 and is probably a background QSO at redshift $z = 0.6$ (Fu et al. 2024); furthermore, its location outside the positional uncertainty of the BAT source leads us to consider it as an unlikely association, leaving source #1 as the most viable identification for 4PBC J0200.8+5423.

4PBC J0258.8+3544

Source position:

- R.A.(J2000) = $02^{h}58^{m}52'.65$
- Dec.(J2000) = $+35^{\circ}44'25''.10$
- Positional uncertainty = $2'.956$

Five XRT observations available:

1. obscode: 00049610001
   observation date: 19/07/2013
   exposure: 476 s
2. obscode: 00049610002
   observation date: 01/08/2013
   exposure: 258 s
3. obscode: 00049610003
   observation date: 07/09/2013
   exposure: 1769 s
4. obscode: 00049610004
   observation date: 08/09/2013
   exposure: 852 s
5. obscode: 00049610005
   observation date: 12/09/2013
   exposure: 1293 s

XRT detects two X–ray sources in the region surrounding 4PBC J0258.8+3544 (see Figure 3):

➢ Source #1, which falls within the BAT error circle, is located at:

R.A.(J2000) = $02^{h}58^{m}46'.73$

Dec.(J2000) = $+35^{\circ}43'58''.40$

error box = $5''.64$

It is detected at 4.0σ and at 3.7σ c.l. in the 0.3–10 keV energy band and above 3 keV, respectively.

Multi–wavelength counterparts to this XRT detection:

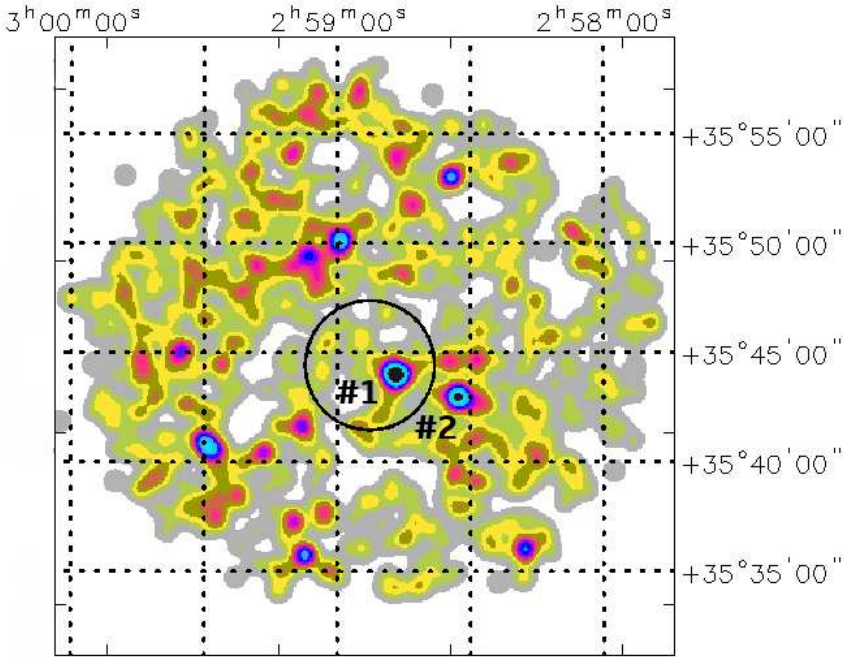

Figure 3: 0.3–10 keV XRT image of the 4PBC J0258.8+3544 field.

- USNO–A2.0 1200–01313992 with magnitudes $B = 14.2$ and $R = 11.4$;
- 2MASS J02584714+3544000 with magnitudes $J = (14.448 \pm 0.067)$, $H = (13.685 \pm 0.078)$, and $K = (13.109 \pm 0.067)$;
- 2MASX J02584733+3543577 with magnitudes $J = (12.516 \pm 0.058)$, $H = (11.819 \pm 0.074)$, and $K = (11.288 \pm 0.072)$;
- AllWISE J025847.30+354357.3 with magnitudes $W1 = (11.718 \pm 0.022)$, $W2 = (11.082 \pm 0.021)$, $W3 = (7.708 \pm 0.019)$, $W4 = (4.956 \pm 0.024)$, and colours ($W1 - W2 = 0.636$, $W2 - W3 = 3.374$) typical of an AGN;
- *Gaia* 140365651563571456 with magnitudes $G = (20.572 \pm 0.027)$, $BP = (18.568 \pm 0.069)$, and $RP = (16.520 \pm 0.043)$
  ($BP - RP = 2.048$);
- GALEX J025846.6+354352 with magnitude $NUV = (20.337 \pm 0.191)$;
- NVSS J025847+354357 with flux density $S(1.4\ \mathrm{GHz}) = (10.3 \pm 0.5)$ mJy;
- VLASS1QLCIR J025847.27+354357.5 with flux $F\mathrm{tot}(2000\text{–}4000\ \mathrm{MHz}) = (6.388 \pm 0.347)$ mJy;
- TGSSADR J025847.2+354357 with flux density $S(150\ \mathrm{MHz}) = (32.7 \pm 6.7)$ mJy;
- RACS–MID J025847.2+354329 with flux $F\mathrm{tot}(1367.5\ \mathrm{MHz}) = 20.8$ mJy;
- RACS–HIGH J025847+35435 with flux $F\mathrm{tot}(1655.5\ \mathrm{MHz}) = 10.1$ mJy.

By modelling the source spectrum with a power law passing through Galactic absorption ($N_{\mathrm{H(Gal)}} = 9.82 \times 10^{20}$ cm^{-2}), we find a photon index $\Gamma = \left(-1.14^{+0.93}_{-1.11}\right)$ and a 2–10 keV flux of $\sim 1.2 \times 10^{-12}$ erg cm^{-2} s^{-1}. If we freeze the photon index to 1.8, the 2–10 keV flux turnes

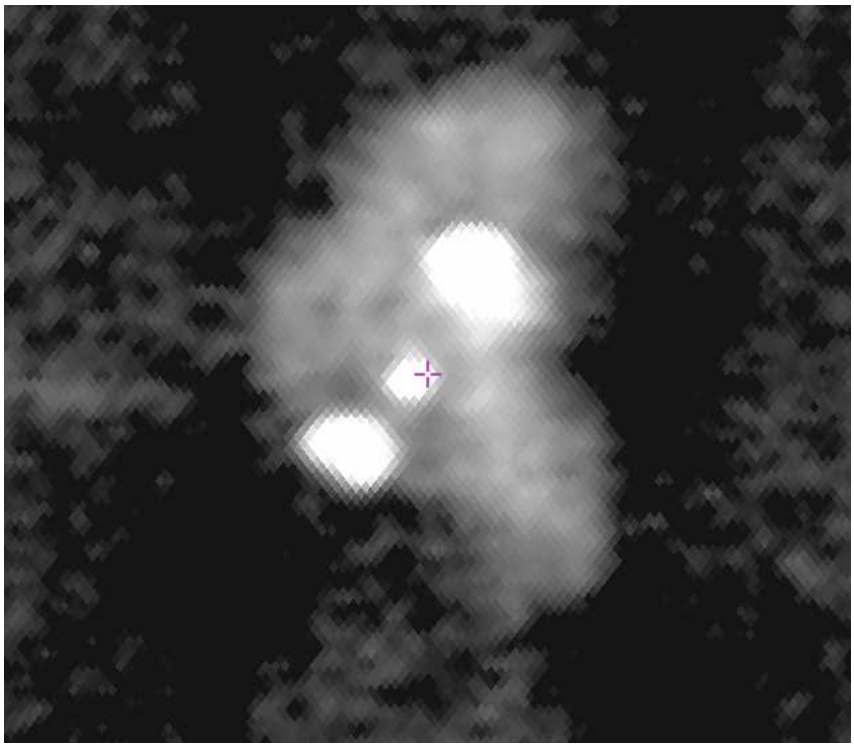

Figure 4: Radio image of source #2 from VLASS.

out to be $\sim 1 \times 10^{-13}$ erg cm^{-2} s^{-1}.

This source is associated with 2MASX J02584733+3543577, classified as a galaxy at redshift $z = (0.04545 \pm 0.00007)$. *AllWISE* colours and radio detection point to a nearby AGN candidate.

➢ Source #2, which lies outside the BAT positional uncertainty, is located at:

R.A.(J2000) = $02^{\rm h}58^{\rm m}32'.63$

Dec.(J2000) = $+35^{\circ}42'55''.27$

error box = $6''.12$

It is detected at 3.4σ and at 2.6σ c.l. in the 0.3–10 keV energy range and above 3 keV, respectively.

Multi–wavelength counterparts to this XRT detection:

- USNO–A2.0 1200–01311665 with magnitudes $B = 20.1$ and $R = 18.2$;

- 2MASS J02583277+3542548 with magnitudes $J = (16.907 \pm 0.173)$, $H = (16.067 \pm 0.211)$, and $K = (14.896 \pm 0.099)$;
- AllWISE J025832.77+354254.7 with magnitudes $W1 = (14.385 \pm 0.029)$, $W2 = (13.719 \pm 0.036)$, $W3 = (11.841 \pm 0.281)$, $W4 = (8.618 \pm 0.000)$, and colours ($W1 - W2 = 0.666$, $W2 - W3 = 1.878$) as expected from an AGN candidate;
- *Gaia* source 140376917262275712 with magnitudes $G = (20.539 \pm 0.015)$, $BP = (20.281 \pm 0.111)$, and $RP = (18.342 \pm 0.041)$
  ($BP - RP = 1.940$);
- NVSS J025832+354300 with flux density $S(1.4\ \mathrm{GHz}) = (396.1 \pm 14.9)$ mJy;
- VLASS1QLCIR J025832.73+354254.7 with flux Ftot(2000–4000 MHz) $= (5.181 \pm 0.374)$ mJy;
- TGSSADR J025832.4+354300 with flux density $S(150\ \mathrm{MHz}) = (1842.1 \pm 184.4)$ mJy;
- RACS–MID J025832.4+354300 with flux Ftot(1367.5 MHz) $= 387.0$ mJy;
- RACS–HIGH J025832+35425 with flux Ftot(1655.5 MHz) $= 336.0$ mJy.

The fit with a power law passing through Galactic absorption ($N_{\mathrm{H(Gal)}} = 9.61 \times 10^{20}$ cm^{-2}) provides a flat photon index $\Gamma = \left(0.48^{+2.89}_{-3.19}\right)$ and a 2–10 keV flux of $\sim 2 \times 10^{-13}$ erg cm^{-2} s^{-1}. If we fix the photon index to 1.8, we estimate a 2–10 keV flux of $\sim 5 \times 10^{-14}$ erg cm^{-2} s^{-1}.

This source (also named B2 0255+35B) is clearly an AGN candidate having the right *AllWISE* colours and radio detection, but it is in the latter waveband that is particularly interesting. It is strong at these low frequencies, variable (Ofek et al. 2011) and polarised (Farnes et al. 2014). However, it is its morphology which is particular, as the source is clearly a radio galaxy with a central core and two prominent lobes, displaying also diffuse emission perpendicular to the lobes, as evident in the VLASS image of the source (see Figure 4). The object is reported with a redshift $z = 0.2$ by Flesch et al. (2024), which suggest a dimension of 87 kpc (lobe to lobe) or almost double overall.

Both source #1 and #2 are probable associations with the BAT emitter, although, on the basis of the X–ray spectral shape, the former is most likely the dominant contributor.

4PBC J0304.6–3026

Source position:

- R.A.(J2000) = $03^{h}04^{m}39'.84$
- Dec.(J2000) = $-30°26'52''.80$
- Positional uncertainty = $4'.13$

Ten XRT observations available:

1. obscode: 00087548001
   observation date: 16/11/2017
   exposure: 128 s
2. obscode: 00087548002
   observation date: 18/11/2017
   exposure: 732 s
3. obscode: 00087548004
   observation date: 22/11/2017
   exposure: 740 s
4. obscode: 00087548005
   observation date: 26/11/2017
   exposure: 1479 s
5. obscode: 00087548006
   observation date: 28/11/2017
   exposure: 348 s
6. obscode: 00087548007
   observation date: 29/11/2017
   exposure: 1798 s
7. obscode: 00087548008
   observation date: 30/11/2017
   exposure: 266 s
8. obscode: 00087548009
   observation date: 01/12/2017
   exposure: 1177 s
9. obscode: 00087548010
   observation date: 04/12/2017
   exposure: 298 s

10. obscode: 00087548011
    observation date: 06/12/2017
    exposure: 512 s

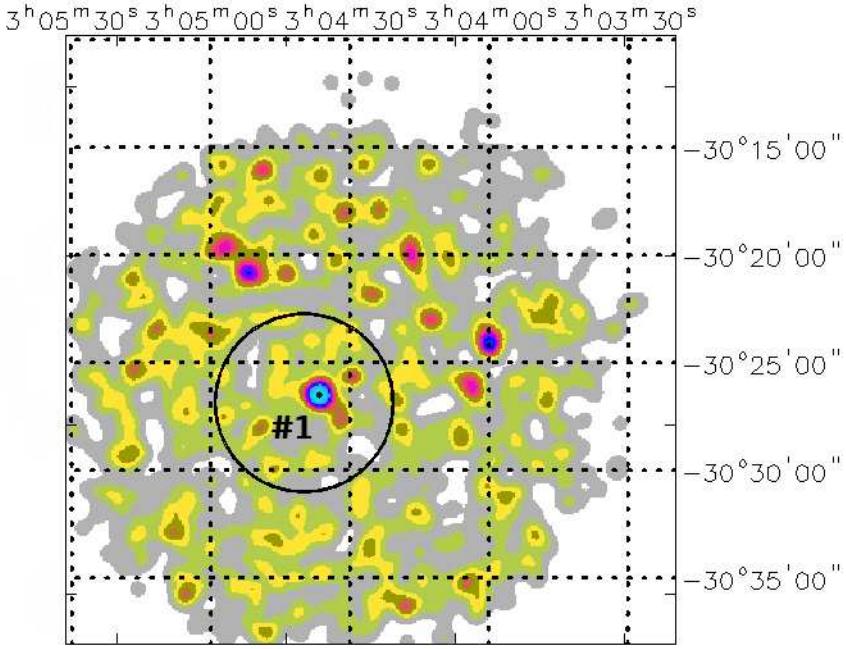

Figure 5: 0.3–10 keV XRT image of the 4PBC J0304.6–3026 field.

XRT detects only one X–ray source within the BAT positional uncertainty (see Figure 5), which is located at:

R.A.(J2000) = $03^{\rm h}04^{\rm m}36'.36$

Dec.(J2000) = $-30^{\circ}26'31''.71$

error box = $4''.90$

It is detected at 5.1σ c.l. in the 0.3–10 keV energy band; no detection is found above 3 keV.

Multi–wavelength counterparts to this XRT detection:

- USNO–A2.0 0525–01040250 with magnitudes $B = 20.2$ and $R = 17.9$;
- AllWISE J030436.50–302631.6 with magnitudes $W1 = (14.715 \pm 0.028)$, $W2 = (14.115 \pm 0.035)$, $W3 = (11.882 \pm 0.182)$, $W4 = (8.847 \pm 0.000)$, and colours typical of an AGN ($W1 - W2 = 0.600$, $W2 - W3 = 2.233$);
- *Gaia* 5058769402155433344 with magnitudes $G = (20.711 \pm 0.009)$, $BP = (20.666 \pm 0.109)$, and $RP = (19.450 \pm 0.057)$
  $(BP - RP = 1.216)$;

- 1eRASS J030436.2–302629 with flux F(0.2–2.3 keV) $\sim 1.4 \times 10^{-13}$ erg cm^{-2} s^{-1};
- MALS J030436.49–302635.7 with flux Ftot(1000 MHz) $= (0.78 \pm 0.30)$ mJy.

A power law passing through Galactic absorption ($N_{\mathrm{H(Gal)}} = 1.40 \times 10^{20}$ cm^{-2}), with a photon index $\Gamma = \left(1.64^{+0.49}_{-0.50}\right)$ and a 2–10 keV flux of $\sim 1.5 \times 10^{-13}$ erg cm^{-2} s^{-1}, provides a good fit to the data.

This source is associated with 2QZ J030436.5–302631, a Seyfert 1 galaxy at redshift $z = 0.436$. The source has the typical near–infrared colours of an AGN and is detected in radio.

4PBC J1626.4–3329

Source position:

- R.A.(J2000) = $16^{\rm h}26^{\rm m}27'.60$
- Dec.(J2000) = $-33^\circ29'27''.60$
- Positional uncertainty = $3'.27$

Seven XRT observations available:

1. obscode: 00087574001
   observation date: 17/01/2018
   exposure: 995 s
2. obscode: 00087574002
   observation date: 18/01/2018
   exposure: 424 s
3. obscode: 00087574003
   observation date: 22/01/2018
   exposure: 853 s
4. obscode: 00087574004
   observation date: 23/01/2018
   exposure: 408 s
5. obscode: 00087574005
   observation date: 24/01/2018
   exposure: 1316 s
6. obscode: 00087574006
   observation date: 28/03/2018
   exposure: 652 s
7. obscode: 00087574008
   observation date: 08/04/2018
   exposure: 574 s

XRT detects an X–ray source within the BAT positional uncertainty (see Figure 6), which is located at:

R.A.(J2000) = $16^{\rm h}26^{\rm m}23'.19$

Dec.(J2000) = $-33^\circ29'32''.73$

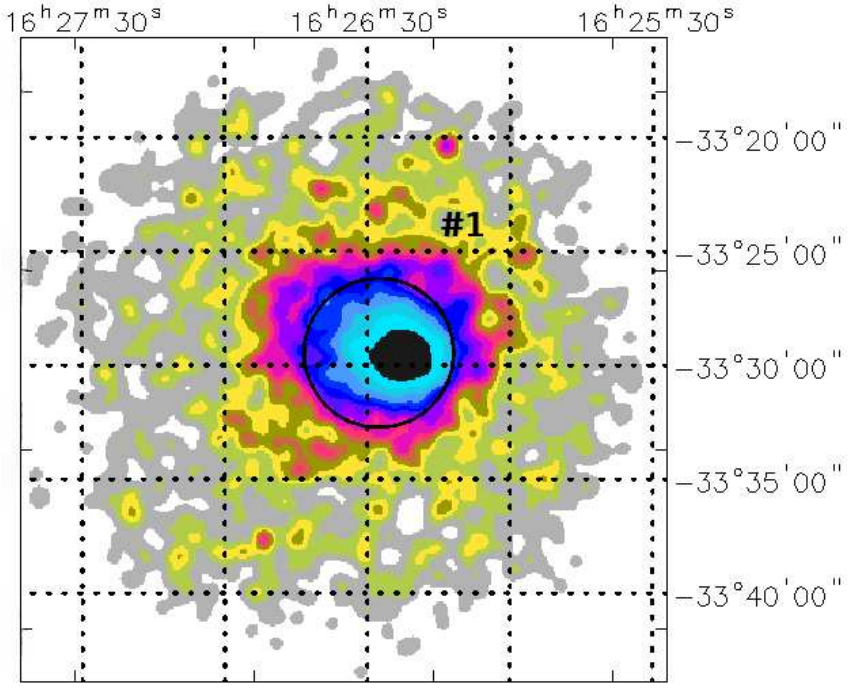

Figure 6: 0.3–10 keV XRT image of the 4PBC J1626.4–3329 field.

error box = 3″.57

It is detected at 28.2σ c.l. in the 0.3–10 keV energy band and at 13.2σ c.l. above 3 keV.

This source is atypical among our set of high–energy emitters, as it is clearly extended in X–rays. This is confirmed by *eROSITA* observations: the source is detected up to the hard X–ray band (1eRASS J162623.0–332940 and SRGA J162626.2–3329, Pavlinsky et al. 2022) with fluxes in the range $(4-5)\times10^{-12}$ erg cm^{-2} s^{-1} and clear extended emission, as evident in Figure 7. The source is quite bright and, as such, reported in many X–ray catalogues such the early *ROSAT* Bright (1RXS J162620.7–332925) and the Rossi X–ray Timing Explorer (*RXTE*) (XSS J16265–3303, Revnivtsev et al. 2004) surveys to the more recent Monitor of All–Sky X–ray Image *MAXI* (2MAXI J1626–333, Hiroi et al. 2013) and *XMM–Newton* Slew (XMMSL3 J162624.7–332949, Saxton et al. 2008) surveys. The X–ray extension provides a clear clue to the source nature, which is associated with a cluster of galaxies CIZA J1626.3–3329, at redshift $z = 0.1098$ (Ebeling et al. 2002), located behind the Milky Way. The source radius is roughly 1 Mpc and its total mass is around 5×10^{14} M$_\odot$ (Piffaretti et al 2011).

The fit with a power law passing through Galactic absorption ($N_{\rm H(Gal)} = 1.88\times10^{21}$ cm^{-2}) does not provide a good fit to the data, as the data–to–model ratio indicates the presence of intrinsic absorption. The addition of this component is required at $>$ 99.99% c.l. and yields an intrinsic column density $N_{\rm H(int)} = \left(0.31^{+0.10}_{-0.08}\right)\times10^{22}$ cm^{-2}; the photon index is $\Gamma = (1.65\pm0.15)$, while the 2–10 keV flux is $\sim$1.5 $\times$ 10^{-11} erg cm^{-2} s^{-1} (see Figure 8). Since this is a cluster of galaxies, we also tried to fit the X–ray spectrum with a bremmstrahlung model. Also in this case the data require extra absorption $N_{\rm H(int)} = \left(0.24^{+0.07}_{-0.06}\right)\times10^{22}$ cm^{-2}. The temperature of the bremsstrahlung com-

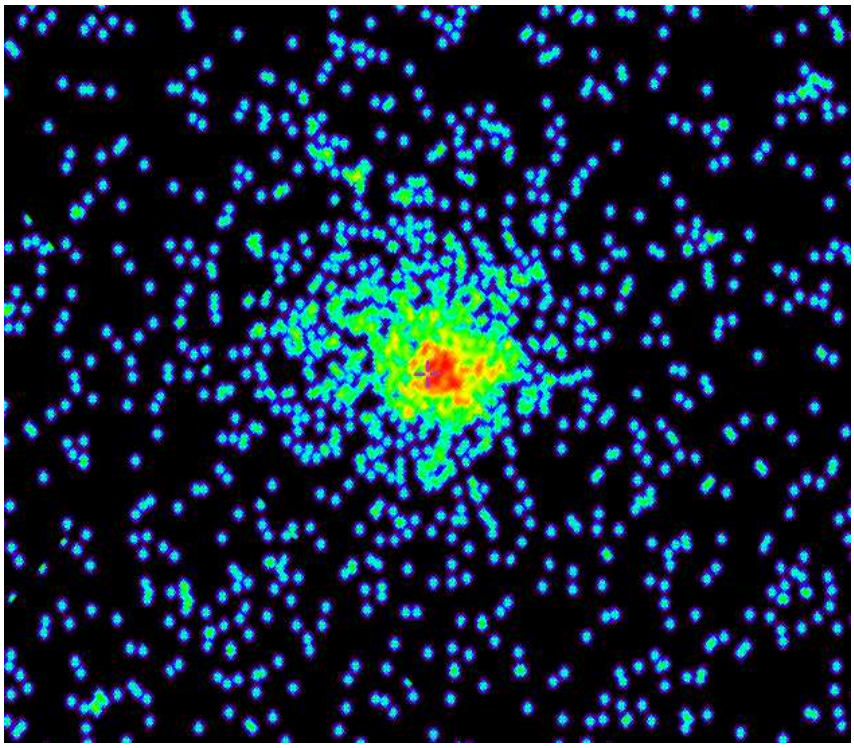

Figure 7: The 0.6–2.3 keV *eROSITA* image of source #1.

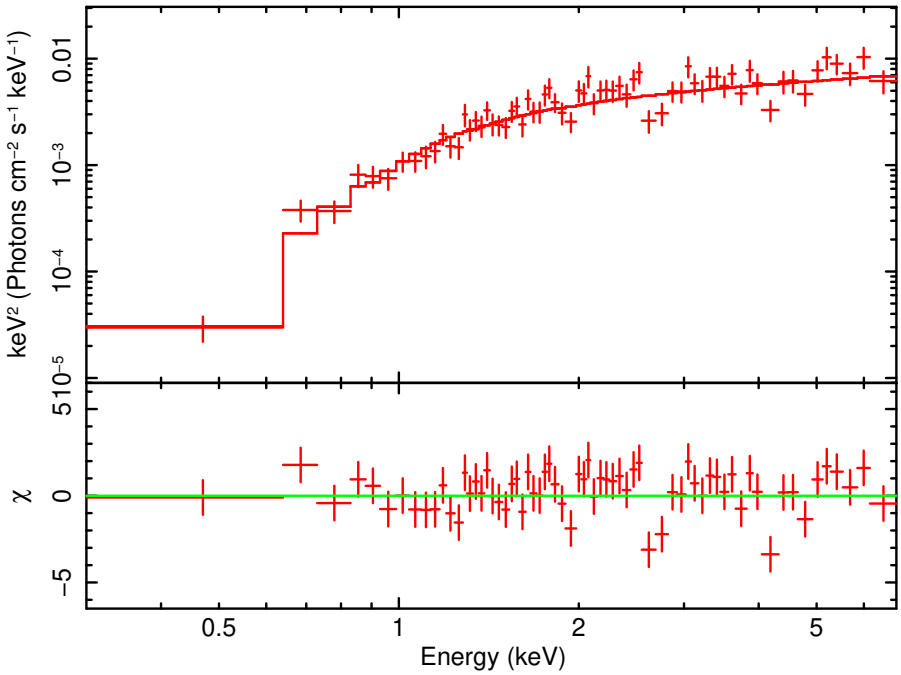

Figure 8: XRT spectrum of source #1 fitted with a power–law model plus Galactic and intrinsic absorption. The residuals from the fit are shown in the bottom panel. See text for details.

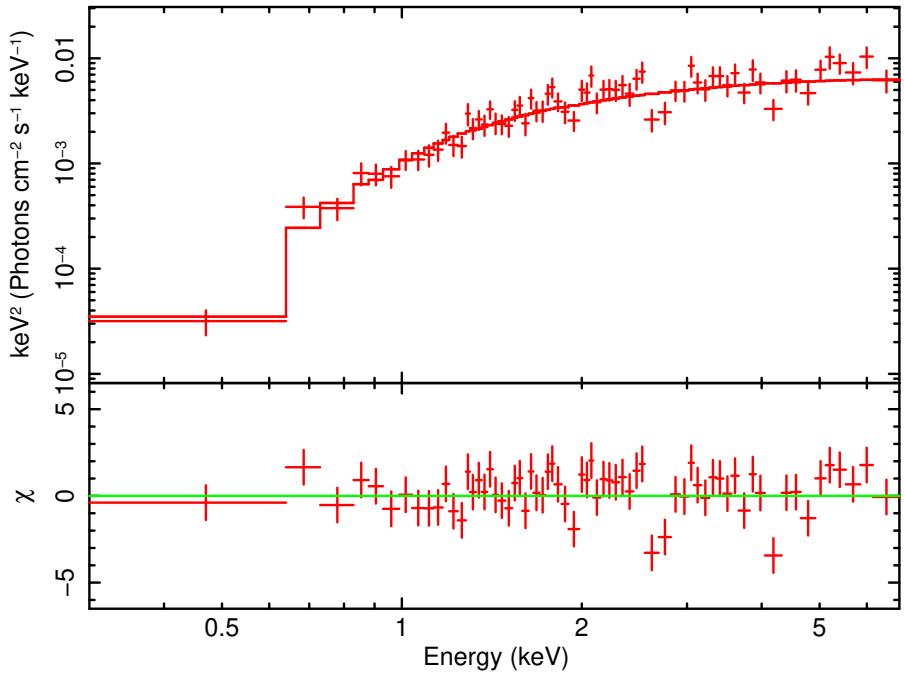

Figure 9: XRT spectrum of source #1 fitted with a bremsstrahlung model plus Galactic and intrinsic absorption. The residuals from the fit are shown in the bottom panel. See text for details.

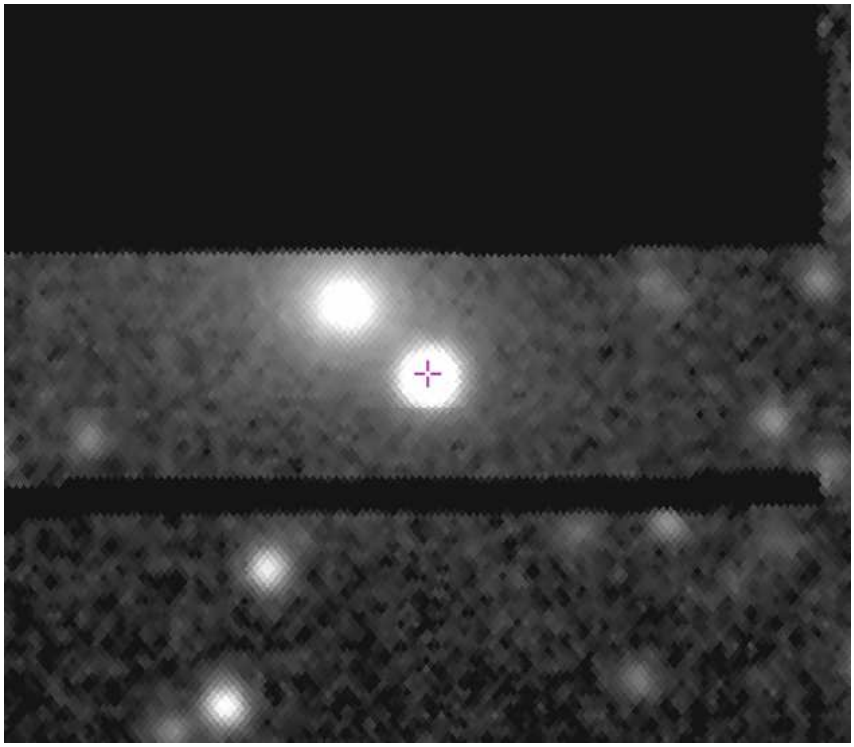

Figure 10: Optical image of source #1 from DECaPS.

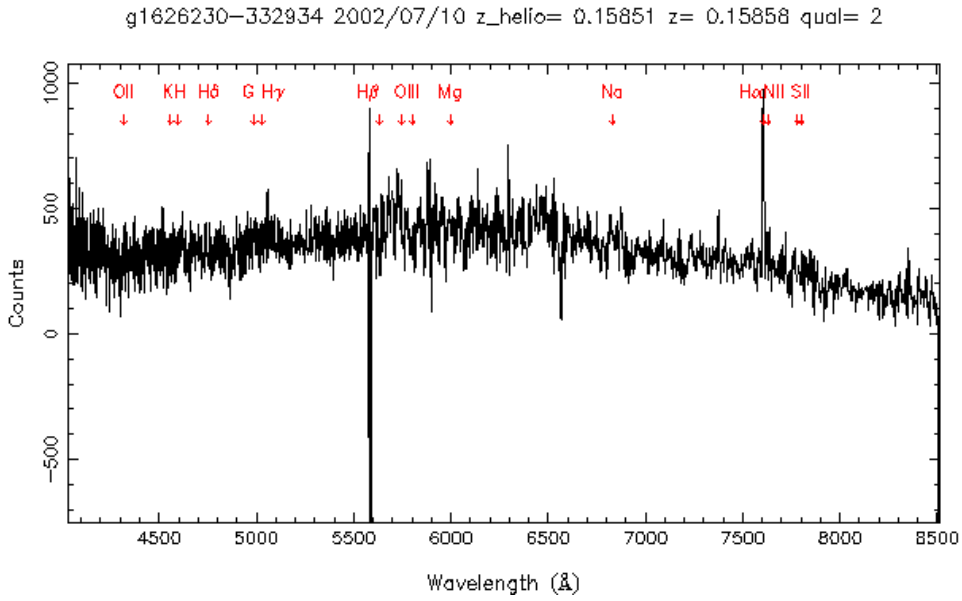

Figure 11: Optical spectrum of source #1 from the 6dF Galaxy Survey.

ponent is $kT = \left(10.0^{+7.1}_{-3.0}\right)$ keV, while the 2–10 keV flux is $\sim 1.4 \times 10^{-11}$ erg cm^{-2} s^{-1} (see Figure 9). In both fit, the spectral feature around 2.4 keV is due to the Au–M intrumental edge, which may be visible in sources with good statistics.

Interestingly, at the best XRT position (brightest part of the cluster or a galaxy?), we find a bright radio source detected by many surveys:

- NVSS J162622–332934 with flux density $S(1.4\ \mathrm{GHz}) = (21.8 \pm 0.8)$ mJy;
- SUMSS J162623–332934 with flux density $S(1.4\ \mathrm{GHz}) = (41.8 \pm 2.1)$ mJy;
- TGSSADR J162623.0–332935 with flux density $S(150\ \mathrm{MHz}) = (181.8 \pm 19.1)$ mJy;
- GLEAM J162623–332933 with flux density Stot(147–154 MHz) = 239.459 mJy and spectral index $\alpha = -1.376$ over the entire GLEAM bandwidth (72–231 MHz) (Hurley–Walker et al. 2017);
- VLASS1QLCIR J162623.22–332931.1 with flux Ftot(2000–4000 MHz) $= (1.484 \pm 0.171)$ mJy;
- VLASS1QLCIR J162623.04–332932.5 with flux Ftot(2000–4000 MHz) $= (2.330 \pm 0.264)$ mJy.

The VLASS survey is able to resolve the emission into two objects (see above), which may be related to two optical sources resolved only in the DECaPS image (as shown in Figure 10), as they are only few arcsec away (4–5″). This clearly complicates the picture, since it is difficult to associate other information with just one of the two sources: for example, the 2MASS Extended object 2MASX J16262295–3329337 might be associated either with one of the two objects or with the combination of the two. Similarly, the 6dF spectrum available in this small region (6dFGS

g1626230–332933, see Figure 11) could be related to either objetcs, although in both cases the southern source seems to be the best association in both cases due to its proximity to both 2MASX J16262295–3329337 and 6dFGS g1626230–332933. If true, the source might be a background QSO at redshift $z = 0.158$ associated, in Simbad, with [CGI2005] 16 and wrongly mistaken with the X–ray binary/microquasar candidate MCQC J1626–33, which clearly cannot be a Galactic object at the source redshift. The fact that it is located within (or behind) the galaxy cluster, in concidence with the brightest part of the X–ray emission, raises also the possibility that it could be an important component of the radiation associated with 4PBC J1626.4–3329.
Only a future observation with *NuSTAR* could possibly shed light on this issue.

4PBC J1630+2680

Source position:

- R.A.(J2000) = $16^{\rm h}30^{\rm m}01'.20$
- Dec.(J2000) = $+26^{\circ}09'00''.00$
- Positional uncertainty = $3'.13$

Four XRT observations available:

1. obscode: 00082248001
   observation date: 12/11/2013
   exposure: 532 s
2. obscode: 00082248002
   observation date: 14/11/2013
   exposure: 3587 s
3. obscode: 00082248003
   observation date: 15/11/2013
   exposure: 3790 s
4. obscode: 00082248004
   observation date: 17/11/2013
   exposure: 2888 s

XRT detects an X–ray source just outside the BAT positional uncertainty (see Figure 12), which is located at:

R.A.(J2000) = $16^{\rm h}30^{\rm m}14'.85$

Dec.(J2000) = $+26^{\circ}12'20''.82$

error box = $4''.60$

It is detected at 5.8σ c.l. in the 0.3–10 keV energy band and at 5.2σ c.l. above 3 keV.

Multi–wavelength counterparts to this XRT detection:

- USNO–A2.0 1125–07670487 with magnitudes $B = 15.8$ and $R = 14.1$;
- 2MASS J16301463+2612233 with magnitudes $J = (14.810 \pm 0.066)$, $H = (13.997 \pm 0.065)$, and $K = (13.118 \pm 0.042)$;
- 2MASX J16301463+2612233 with magnitudes $J = (14.007 \pm 0.063)$, $H = (13.299 \pm 0.080)$, and $K = (12.647 \pm 0.071)$;

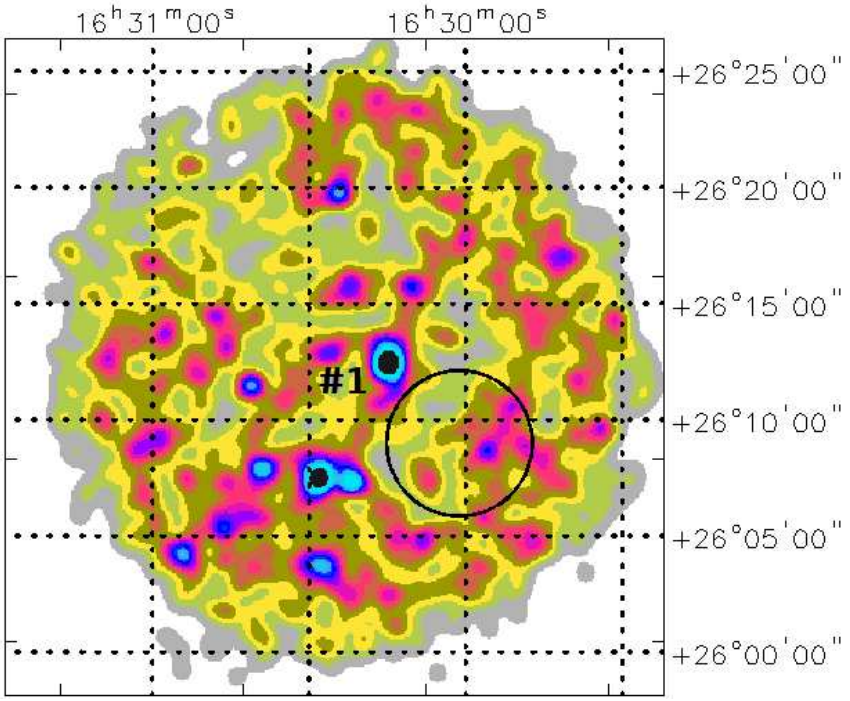

Figure 12: 0.3–10 keV XRT image of the 4PBC J1630.0+2680 field.

- AllWISE J163014.63+261223.3 with magnitudes $W1 = (11.498 \pm 0.119)$, $W2 = (10.558 \pm 0.021)$, $W3 = (7.683 \pm 0.019)$, $W4 = (5.329 \pm 0.042)$, and colours ($W1 - W2 = 0.94$, $W2 - W3 = 2.875$) typical of and AGN;
- *Gaia* 1304221696227588736 with magnitudes $G = (20.206 \pm 0.028)$, $BP = (17.821 \pm 0.023)$, and $RP = (16.486 \pm 0.008)$
  ($BP - RP = 1.334$);
- GALEX J163014.5+261222 with magnitudes $FUV = (20.372 \pm 0.205)$ and $NUV = (19.360 \pm 0.081)$;
- FIRST J163014.6+261223 with flux density $S(1.4\ \mathrm{GHz}) = (7.25 \pm 0.14)$ mJy;
- VLASS1QLCIR J163014.64+261223.3 with flux Ftot(2000–4000 MHz) $= (3.615 \pm 0.294)$ mJy;
- VLASS1QLCIR J163014.62+261223.4 with flux Ftot(2000–4000 MHz) $= (3.479 \pm 0.533)$ mJy;
- RACS–MID J163014.6+261223 with flux Ftot(1367.5 MHz) = 7.89 mJy;
- RACS–HIGH J163014+26122 with flux Ftot(1655.5 MHz) = 6.2 mJy.

The fit with a power law passing through Galactic absorption ($N_{\mathrm{H(Gal)}} = 3.39 \times 10^{20}$ cm^{-2}) indicates a flat photon index $\Gamma = \left(-0.50^{+0.56}_{-0.74}\right)$ and a 2–10 keV flux of $\sim 1.1 \times 10^{-12}$ erg cm^{-2} s^{-1}. If we fix the photon index to 1.8, the data require extra absorption $N_{\mathrm{H(int)}} = \left(3.94^{+8.54}_{-2.26}\right) \times 10^{22}$ cm^{-2}; the 2–10 keV flux is $\sim 4.4 \times 10^{-13}$ erg cm^{-2} s^{-1}.

The source is identified with LEDA 3866904, classified as a LINER–type galaxy at redshift $z = (0.13146 \pm 0.00001)$. The source activity is underlined by its *AllWISE* colours and radio detection; it is also reported as variable at 1.4 GHz from the comparison between NVSS and FIRST data sets (Ofek et al. 2011). It is listed, as galaxy with uncertain classification (Starburst galaxy/LINER), in the Mapping Nearby Galaxies at Apache Point Observatory (MaNGA) Survey maybe due to AGN flickering (Comerford et al. 2022); in this scenario, the spatially extended AGN emission (traced by [OIII]) may be left over from past AGN activity (e.g., Eracleous et al. 1995; Lintott et al. 2009), while the central AGN emission (traced by hard X–rays) may be a sign of current AGN activity.

4PBC J1638.8–1413

Source position:

- R.A.(J2000) = $16^{\rm h}38^{\rm m}49'.44$
- Dec.(J2000) = $-14^{\circ}13'44''.40$
- Positional uncertainty = $3'.16$

Five XRT observations available:

1. obscode: 00094029001
   observation date: 27/04/2018
   exposure: 1459 s
2. obscode: 00094029002
   observation date: 29/04/2018
   exposure: 648 s
3. obscode: 00094029003
   observation date: 26/05/2018
   exposure: 913 s
4. obscode: 00094029004
   observation date: 02/06/2018
   exposure: 728 s
5. obscode: 00094029006
   observation date: 18/06/2018
   exposure: 1811 s

The only X–ray source detected by XRT within the BAT positional uncertainty (see Figure 13) is located at:

R.A.(J2000) = $16^{\rm h}38^{\rm m}45'.29$

Dec.(J2000) = $-14^{\circ}15'48''.68$

error box = $3''.65$

It is detected at 22.7σ c.l. in the 0.3–10 keV energy range and at 12.2σ c.l. above 3 keV.

Multi–wavelength counterparts to this XRT detection:

- USNO–A2.0 0750–09900118 with magnitudes $B = 17.1$ and $R = 16.3$;

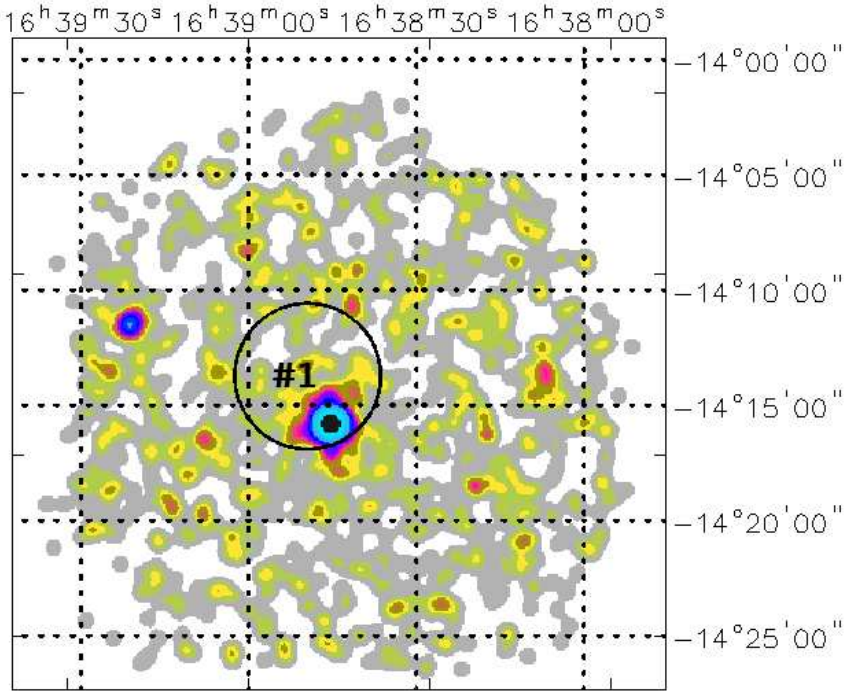

Figure 13: 0.3–10 keV XRT image of the 4PBC J1638.8–1413 field.

- 2MASS J16384528–1415502 with magnitudes $J = (15.137 \pm 0.054)$, $H = (14.060 \pm 0.041)$, and $K = (12.982 \pm 0.035)$;
- AllWISE J163845.28–141550.2 with magnitudes $W1 = (11.244 \pm 0.024)$, $W2 = (10.089 \pm 0.020)$, $W3 = (7.506 \pm 0.020)$, $W4 = (5.178 \pm 0.036)$, and colours ($W1 - W2 = 1.155$, $W2 - W3 = 2.583$) typical of an AGN;
- *Gaia* 4327083966226367104 with magnitudes $G = (16.937 \pm 0.004)$, $BP = (17.471 \pm 0.011)$, and $RP = (16.080 \pm 0.008)$
  ($BP - RP = 1.391$);
- 1RXS J163845.7–141553 with flux F(0.2–2.4 keV) $= 6.03 \times 10^{-12}$ erg cm^{-2} s^{-1};
- NVSS J163845–141551 with flux density S(1.4 GHz) $= (969.5 \pm 32.0)$ mJy;
- VLASS1QLCIR J163845.28–141549.9 with flux Ftot(2000–4000 MHz) $= (203.696 \pm 0.909)$ mJy;
- RACS–MID J163845.7–141554 with flux Ftot(1367.5 MHz) $= 924.0$ mJy;
- RACS–HIGH J163845–14155 with flux Ftot(1655.5 MHz) $= 809.0$ mJy.

The fit with a power law passing through Galactic absorption ($N_{\rm H(Gal)} = 1.44 \times 10^{21}$ cm^{-2}) does not provide a good fit to the data, as the residuals indicate the presence of intrinsic absorption; the addition of this component is required by the data at $> 99.99\%$ c.l.. The best–fit parameters are the following: $N_{\rm H(int)} = \left(0.18^{+0.09}_{-0.07}\right) \times 10^{22}$ cm^{-2}, $\Gamma = \left(1.71^{+0.23}_{-0.21}\right)$, while the 2–10 keV flux is $\sim 5.5 \times 10^{-12}$ erg cm^{-2} s^{-1}.

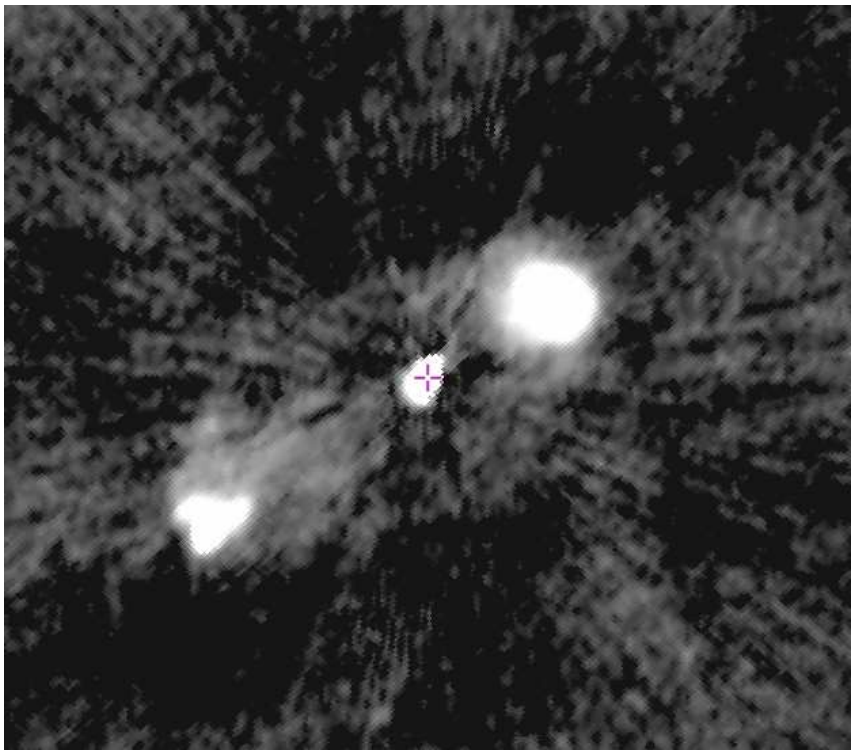

Figure 14: Radio image of source #1 from VLASS.

This source is associated with the quasar QSO B1635–014, also PKS J1638–1415, having a spectroscopic redshift $z = (0.2575 \pm 0.0004)$. It is radio variable, as indicated by a comparison between NVSS and FIRST data sets (Ofek et al. 2011), and is also polarised at the same frequencies (Farnes et al. 2014). Although these properties suggest it might be a blazar candidate, its radio morphology is typical of a radio galaxy with a bright central nucleus and two prominent radio lobes (see Figure 14 from VLASS). The source overall dimension is around $1'.7$, which at the source distance turns into a 400 kpc extension (4 kpc/arcseconds).

4PBC J1735.9–1528

Source position:

- R.A.(J2000) = $17^{\rm h}35^{\rm m}55'.44$
- Dec.(J2000) = $-15^{\circ}28'37''.20$
- Positional uncertainty = $2'.78$

Four XRT observations available:

1. obscode: 00087582001
   observation date: 02/02/2018
   exposure: 2174 s
2. obscode: 00087582002
   observation date: 05/02/2018
   exposure: 2174 s
3. obscode: 00087582003
   observation date: 06/02/2018
   exposure: 1068 s
4. obscode: 00087582004
   observation date: 08/02/2018
   exposure: 2273 s

XRT detects only one X–ray source within the BAT positional uncertainty (see Figure 15), which is located at:

R.A.(J2000) = $17^{\rm h}36^{\rm m}00'.82$

Dec.(J2000) = $-15^{\circ}29'45''.66$

error box = $3''.61$

It is detected at 26.3σ and 13.0σ c.l. in the 0.3–10 keV energy range and above 3 keV, respectively.

Multi–wavelength counterparts to this XRT detection:

- USNO–A2.0 0675–20563919 with magnitudes $B = 16.9$ and $R = 16.1$;
- 2MASS J17360070–1529466 with magnitudes $J = (14.708 \pm 0.063)$, $H = (13.756 \pm 0.058)$, and $K = (12.668 \pm 0.043)$;
- 2MASX J17360068–1529464 with magnitudes $J = (14.131 \pm 0.171)$, $H = (13.127 \pm 0.144)$, and $K = (12.338 \pm 0.094)$;

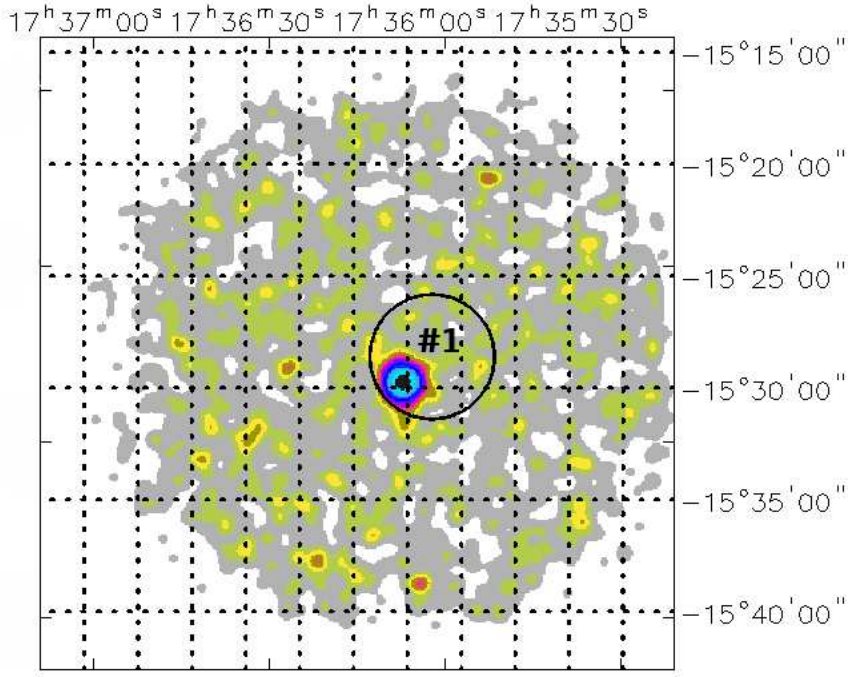

Figure 15: 0.3–10 keV XRT image of the 4PBC J1735.9–1528 field.

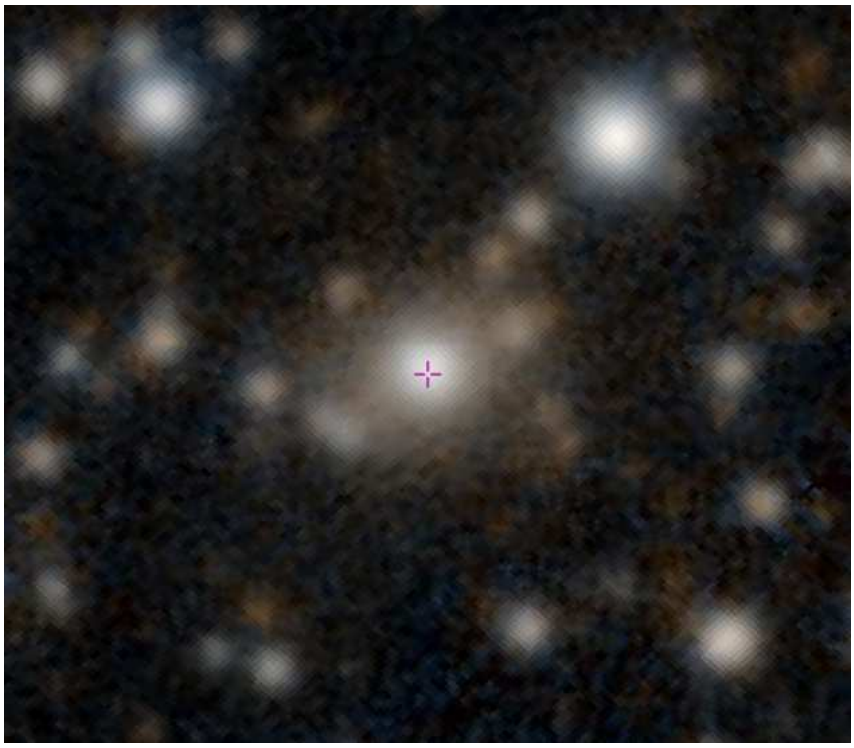

Figure 16: Optical image of source #1 from Pan–STARRS.

- AllWISE J173600.69–152946.6 with magnitudes $W1 = (10.997 \pm 0.022)$, $W2 = (9.957 \pm 0.020)$, $W3 = (7.249 \pm 0.018)$, $W4 = (4.967 \pm 0.033)$, and colours typical of an AGN ($W1 - W2 = 1.04$, $W2 - W3 = 2.708$);
- *Gaia* 4125085194710985984 with magnitudes $G = (17.496 \pm 0.009)$, $BP = (17.828 \pm 0.021)$, and $RP = (16.233 \pm 0.019)$
  $(BP - RP = 1.595699)$.

The fit with a power law passing through Galactic absorption ($N_{\mathrm{H(Gal)}} = 2.10 \times 10^{21}$ cm^{-2}) is a good fit to the data, providing a photon index $\Gamma = (1.59 \pm 0.10)$ and a 2–10 keV flux of $\sim 6.8 \times 10^{-12}$ erg cm^{-2} s^{-1}.

Although no radio emission has yet been associated with this source, its *AllWISE* colours and optical extension, typical of a galaxy (see Figure 16), point to an AGN candidate (see also Edelson et al. 2012 and Kouzuma et al. 2010); no redshift is available for the object.

4PBC J1824.5+2054

Source position:

- R.A.(J2000) = $18^h24^m33'.12$
- Dec.(J2000) = $+20°54'14''.40$
- Positional uncertainty = $2'.88$

Three XRT observations available:

1. obscode: 00085328001
   observation date: 08/11/2014
   exposure: 1850 s
2. obscode: 00085328002
   observation date: 16/11/2014
   exposure: 336 s
3. obscode: 00085328003
   observation date: 18/11/2014
   exposure: 737 s

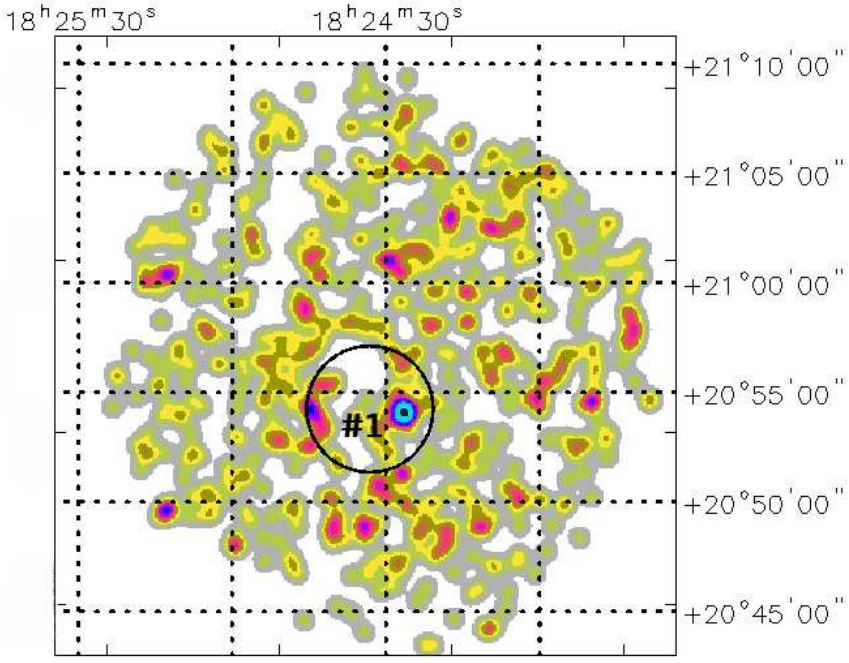

Figure 17: 0.3–10 keV XRT image of the 4PBC J1824.5+2054 field.

XRT detects only one X–ray source within the BAT positional uncertainty (see Figure 17), which is located at:

R.A.(J2000) = $18^{\rm h}24^{\rm m}26'.59$

Dec.(J2000) = $+20^{\circ}54'05''.79$

error box = $6''.12$

It is detected at 3.7σ and 3.6σ c.l. in the 0.3–10 keV energy range and above 3 keV, respectively.

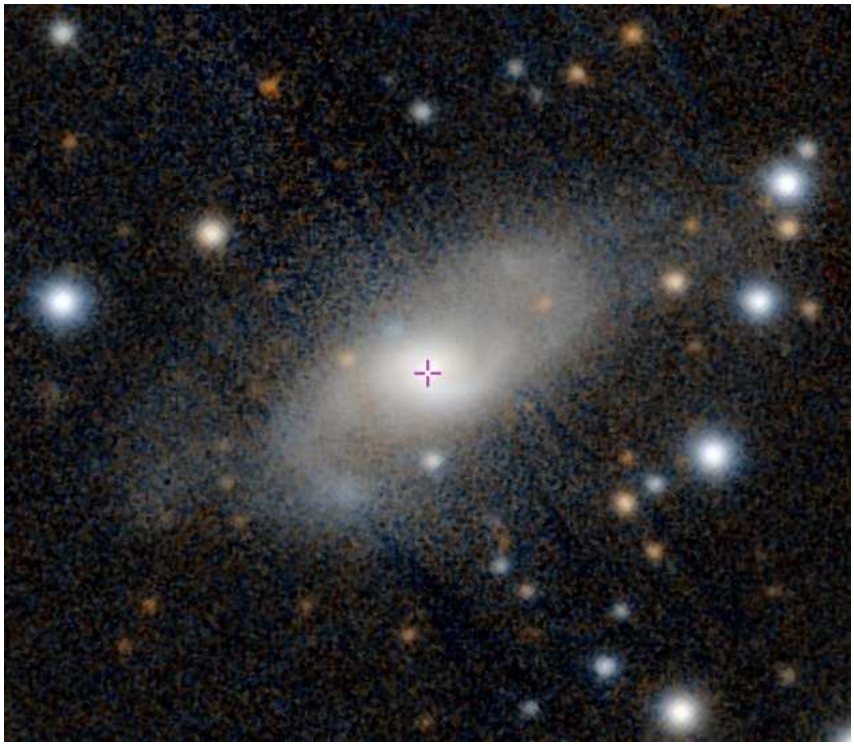

Figure 18: Optical image of source #1 from Pan–STARRS.

Multi–wavelength counterparts to this XRT detection:

- USNO–A2.0 1050–10424216 with magnitudes $B = 12.2$ and $R = 10.5$;
- 2MASS J18242656+2054091 with magnitudes $J = (13.474 \pm 0.048)$, $H = (12.716 \pm 0.061)$, and $K = (12.304 \pm 0.044)$;
- 2MASX J18242659+2054092 with magnitudes $J = (11.851 \pm 0.043)$, $H = (11.058 \pm 0.053)$, and $K = (10.924 \pm 0.069)$;
- AllWISE J182426.56+205409.0 with magnitudes $W1 = (11.174 \pm 0.023)$, $W2 = (10.784 \pm 0.020)$, $W3 = (7.046 \pm 0.016)$, $W4 = (4.354 \pm 0.023)$, and colours ($W1 - W2 = 0.390$, $W2 - W3 = 3.738$);

- *Gaia* 4528609874770164096 with magnitudes $G = (18.934 \pm 0.011)$, $BP = (16.829 \pm 0.008)$, and $RP = (15.349 \pm 0.004)$
  $(BP - RP = 1.480)$;
- NVSS J182426+205408 with flux density $S(1.4\ \mathrm{GHz}) = (16.1 \pm 0.6)$ mJy;
- VLASS1QLCIR J182426.56+205409.2 with flux $F\mathrm{tot}(2000\text{–}4000\ \mathrm{MHz}) = (6.912 \pm 0.294)$ mJy;
- TGSSADR J182426.4+205408 with flux density $S(150\ \mathrm{MHz}) = (31.1 \pm 5.6)$ mJy;
- RACS–MID J182426.5+205411 with flux $F\mathrm{tot}(1367.5\ \mathrm{MHz}) = 17.5$ mJy;
- RACS–HIGH J182426+20541 with flux $F\mathrm{tot}(1655.5\ \mathrm{MHz}) = 22.6$ mJy.

Due to the poor statistical quality of the X–ray data, we can only infer a 2–10 keV flux of $\sim 1 \times 10^{-13}$ by assuming a power law passing through Galactic absorption ($N_{\mathrm{H(Gal)}} = 1.38 \times 10^{21}\ \mathrm{cm}^{-2}$) with the photon index frozen to 1.8.

The source is identified with Z 114–5/LEDA 61838, an AGN candidate at redshift $z = (0.016742 \pm 0.000123)$. It is a spiral galaxy not yet optically classified (see Figure 18); the near–infraed colours suggest either a low luminosity AGN (like a LINER) or an absorbed source. Follow–up observations with *Chandra* and *XMM–Newton* suggest the source might be an obscured Compton–thin AGN (X–ray column density just below $10^{24}\ \mathrm{cm}^{-2}$, Cox et al. 2025), thus providing an explanation for the atypical *AllWISE* colours.

4PBC J2201.3+7546

Source position:

- R.A.(J2000) = $22^{h}01^{m}21'.51$
- Dec.(J2000) = $+75°46'11''.20$
- Positional uncertainty = $2'.86$

Three XRT observations available:

1. obscode: 00046328001
   observation date: 25/06/2012
   exposure: 587 s
2. obscode: 00046328002
   observation date: 01/07/2012
   exposure: 1587 s
3. obscode: 00046328003
   observation date: 03/07/2012
   exposure: 2221 s

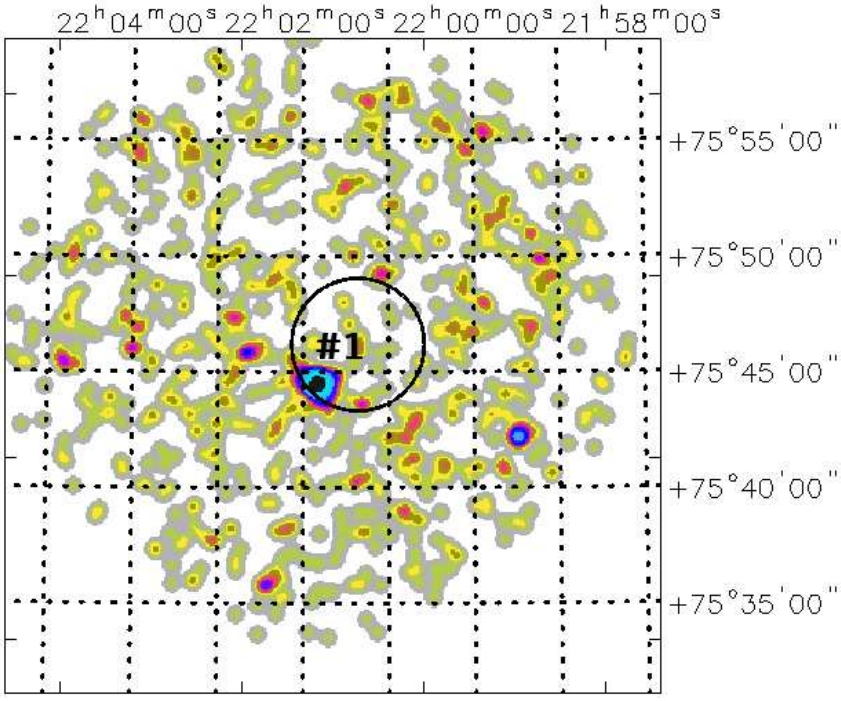

Figure 19: 0.3–10 keV XRT image of the 4PBC J2201.2+7546 field.

XRT detects only one X–ray source within the BAT error circle (see Figure 19), which is located at:

R.A.(J2000) = $22^{\rm h}01^{\rm m}49'.84$

Dec.(J2000) = $+75^{\circ}44'29''.37$

error box = $3''.94$

It is detected at 12.0σ c.l. in the 0.3–10 keV energy band and at 7.9σ c.l. above 3 keV.

Multi–wavelength counterparts to this XRT detection:

- USNO–A2.0 1650–02488725 with magnitudes $B = 18.6$ and $R = 16.7$;
- 2MASS J22014980+7544287 with magnitudes $J = (14.707 \pm 0.054)$, $H = (13.749 \pm 0.061)$, and $K = (12.985 \pm 0.038)$;
- 2MASX J22014968+7544286 with magnitudes $J = (14.340 \pm 0.104)$, $H = (13.247 \pm 0.091)$, and $K = (12.679 \pm 0.095)$;
- AllWISE J220149.81+754428.7 with magnitudes $W1 = (11.897 \pm 0.023)$, $W2 = (10.970 \pm 0.021)$, $W3 = (7.818 \pm 0.021)$, $W4 = (5.225 \pm 0.029)$, and colours typical of an AGN candidate ($W1 - W2 = 0.927$, $W2 - W3 = 3.152$);
- *Gaia* 2280216661642677632 with magnitudes $G = (18.266 \pm 0.007)$, $BP = (18.531 \pm 0.023)$, and $RP = (16.433 \pm 0.010)$
  ($BP - RP = 2.098$);
- VLASS1QLCIR J220149.87+754428.4 with flux Ftot(2000–4000 MHz) $= (1.864 \pm 0.202)$ mJy.

The fit with a power law passing through Galactic absorption ($N_{\rm H(Gal)} = 1.51 \times 10^{21}$ cm^{-2}) provides a flat photon index $\Gamma = \left(0.79^{+0.23}_{-0.24}\right)$ and a 2–10 keV flux of $\sim 3.8 \times 10^{-12}$ erg cm^{-2} s^{-1}. However, if we freeze the photon index to 1.8, the data show evidence of extra absorption $N_{\rm H(int)} = \left(0.63^{+0.34}_{-0.25}\right) \times 10^{22}$ cm^{-2}; the 2–10 keV flux is $\sim 2.3 \times 10^{-12}$ erg cm^{-2} s^{-1}.

In Simbad and NED the source is reported as 2MASS J22014980+7544287/WISEA J220149.81+754428.7, an AGN candidate at redshift $z = 0.037638$ (Bilicki et al. 2014), although Flesch (2024) and Fu et al. (2024) provide a higher redshift ($z \sim 0.5$). Clearly, follow–up optical observations can solve this issue and provide a proper classification for the source.

Bibliography

[1] Bianchi L., Herald J., Efremova B., et al. 2011, Ap&SS, 335, 161

[2] Bilicki M., Jarrett T. H., Peacock J. A., et al. 2014, ApJS, 210, 9

[3] Cash W. 1979, ApJ, 228, 939

[4] Chambers K. C., Magnier E. A., Metcalfe N., et al., 2016, arXiv:1612.05560

[5] Comerford J. M., Negus J., Barrows R. S., et al. 2022, ApJ, 927, 23

[6] Condon J. J., Cotton W. D., Greisen E. W., et al. 1998, AJ, 115, 1693

[7] Cox I. S., Torres–Albá N., Marchesi S., et al. 2024, ApJ, 979, 130

[8] Cutri R. M., Wright E. L., Conrow T., et al. 2013, `https://wise2.ipac.caltech.edu/docs/release/allwise/expsup/index.html`

[9] Dabhade, P., Mahato M., Bagchi J., et al. 2020, A&A, 642, A153

[10] Deka P. P., Gupta N., Jagannathan P., et al. 2024, ApJS, 270, 33

[11] Duchesne S. W., Ross K., Thomson A. J. M., et al. 2025, PASA, 42, e038

[12] Duchesne S. W., Grundy, J. A., Heald G. H., et al. 2024, PASA, 41, e003

[13] Duncan K. J. 2022, MNRAS, 512, 3662

[14] Ebeling H., Mullis C. R., & Tully R. B. 2002, ApJ, 580, 774

[15] Edelson R. & Malkan M. 2012, ApJ, 751, 52

[16] Eracleous M., Livio M., Halpern J. P., & Storchi–Bergmann T. 1995, ApJ, 438, 610

[17] Farnes J. S., Gaensler B. M., & Carretti E. 2014, ApJS, 212, 15

[18] Flesch E. W. 2024, OJAp, 7, 6

[19] Fu Y., Wu X., Yang Q., et al. 2021, ApJS, 254,6

[20] Gaia Collaboration: Brown A. G. A., Vallenari A., Prusti T., et al. 2021, A&A, 649, A1

[21] Gehrels N., Chincarini G., Giommi P., et al. 2004, ApJ, 611, 1005

[22] Gordon Y. A., Boyce M. M., O'Dea C. P., et al. 2021, ApJS, 255, 30

[23] Helfand D. J., White R. L., & Becker R. H. 2015, ApJ, 801, 26

[24] Hill J. E., Burrows D. N., Nousek J. A., et al. 2004, Proc. SPIE, 5165, 217

[25] Intema H. T., Jagannathan P., Mooley K. P., & Frail D. A. 2017, A&A, 598, A78

[26] Jones D. H., Read M. A., Saunders W., et al. 2009, MNRAS, 399, 683

[27] Kalberla P. M. W., Burton W. B., Hartmann D., et al. 2005, A&A, 440, 775

[28] Hiroi K., Ueda Y., Hayashida M., et al. 2013, ApJS, 207, 36
[29] Hurley–Walker N., Callingham J. R., Hancock P. J., et al. 2017, MNRAS, 464, 1146
[30] Kouzuma S. & Yamaoka H. 2010, MNRAS, 405, 2062
[31] Lintott C. J., Schawinski K., Keel W., et al. 2009, MNRAS, 399, 129
[32] Malizia A., Bassani L., Landi R., et al., 2023, A&A, 671, A152
[33] Mauch T., Murphy T., Buttery H. J., et al. 2003, MNRAS, 342, 1117
[34] Merloni A., Lamer G., Liu T., et al. 2024, A&A, 682, A34
[35] Monet D. G., Levine S. E., Canzian B., et al. 2003, AJ, 125, 984
[36] Monet D. G. 1998, AAS, 30, 1427
[37] Ofek E. O., Frail D. A., & Breslauer B. 2011, ApJ, 740, 65
[38] Pavlinsky M., Sazonov S., Burenin R., et al. 2022, A&A, 661, A38
[39] Piffaretti R., Arnaud M., Pratt G. W., et al. 2011, A&A, 534, A109
[40] Revnivtsev M., Sazonov S., Jahoda K., & Gilfanov M. 2004, A&A, 418, 927
[41] Ross K., Hurley–Walker N., Galvin T. J., et al. 2024, PASA, 41, e054
[42] Saxton R. D., Read A. M., Esquej P., et al. 2008, A&A, 480, 611
[43] Schlafly E. F., Green G. M., Lang D., et al. 2018, ApJS, 234, 39
[44] Skrutskie M. F., Cutri R. M., Stiening R., et al. 2006, AJ, 131, 1163
[45] Voges W., Aschenbach B., Boller Th., et al. 1999, A&A, 349, 389
[46] Wright E. L., Eisenhardt P. R. M., Mainzer A. K., et al. 2010, AJ, 140, 1868